Argus: An L-Band All-Sky Astronomical Surveillance System

Steven W. Ellingson, *Senior Member, IEEE*, Grant A. Hampson, and Russell K. Childers

***Abstract*—Argus is an experimental antenna array system designed to demonstrate all-sky monitoring for transient signals in the frequency range 1200–1700 MHz. It currently consists of 22 broadband spiral antennas (expandable to 32) which are individually instrumented, digitized, and analyzed in an attempt to detect and localize both broadband and narrowband astronomical transients. In this paper, we describe the design of the instrument. Notable features include a novel array data aggregation architecture, a detection algorithm which does not require accurate calibration or detailed knowledge of the array manifold, and very low per-element cost of about US$1k/element. A sensitivity of at least $6.6 \times 10^{-22}\ \mathrm{Wm^{-2}\ Hz^{-1}} = 66\ \mathrm{kJy}$ (zenith at 1700 MHz for a 209 ms observation with 60 kHz bandwidth) is achieved for the system as implemented. Performance is demonstrated in an experiment in which the Sun is detected, localized, and tracked as it moves across the sky. Other experiments confirming the functionality of Argus as an all-sky surveillance system are summarized.**

***Index Terms*—Antenna array, direction finding, radio astronomy.**

I. Introduction

TRADITIONAL radio astronomy uses large, filled-aperture antennas, both singly and in arrays, to achieve high sensitivity and spatial resolution [1]. However, such instruments have the disadvantage that they have very narrow field of view (FOV) and can only be pointed in one direction at a time. Furthermore, this approach limits the potential for discovery of new transient astronomical sources, because such sources can potentially be very strong in astronomical terms and yet remain undiscovered simply because no radio telescope happens to be pointed in the right direction during the event. The broadening realization that the radio sky includes many such sources [2] has heightened interest in instruments that can observe large FOV—ideally, the entire sky—continuously. In a 1996 paper, R. S. Dixon of the Ohio State University (OSU) proposed "Argus," a concept for a radio telescope array using a large array of broadband antennas with broad beamwidth that provides all-sky FOV, ability to generate multiple simultaneous beams, and "retroactive observing," i.e., the potential to save raw telescope data in such a way that observing beams can be formed long after the data are collected [3].

An especially tantalizing possibility is that this class of radio transients might include an intermittent beacon transmitted by an extraterrestrial civilization. If another civilization were inclined to transmit such a signal, there are many reasons why an intermittent beacon at radio frequencies, and in L-Band in particular, would be a likely choice [4]. For this reason, the SETI Institute, a leading organization in the search for extraterrestrial intelligence through technical means, considers an "omnidirectional search system" (OSS) to be an important component in a deliberate search for such signals [5]. Recognizing that Argus and OSS were essentially the same concept, the SETI Institute funded a modest effort at OSU over the period 2000–2003 to design and build a small prototype that would demonstrate the essential features of an OSS [6]. The instrument became operational in 2003 and has been operating continuously (except for downtime related to power failures, component replacements, and so on) since that time. This paper summarizes the results of the project.

Argus as it exists today is a fully-operational radio telescope consisting of 22 L-band spiral antennas and associated electronics located on OSU's Columbus, OH campus. The output of each antenna is individually received, downconverted, digitized, and then analyzed in real-time for transients which are either broadband (as expected from astrophysical sources) or narrowband (as expected from beacon candidates). In this paper, we explain the design of Argus (Section II), address theoretical performance (Section III), demonstrate the ability of the system to detect and localize the Sun (Section IV), and summarize other experiments which demonstrate various capabilities of the system (Section V). This paper concludes with a discussion of current activities and includes a brief discussion comparing Argus to other projects with similar goals.

II. System Description

In this section we describe the design of Argus as it exists today. Much of the design is custom; see [6], [7] for additional details.

A. Antenna Array

The array is shown in Fig. 1. It currently consists of 22 operational spiral antennas arranged in the geometry shown in Fig. 2. The size of the elements precludes Nyquist sampling of the aperture, so to help mitigate aliasing a pseudorandom arrangement of elements is chosen. The minimum dimension of the array is

Manuscript received May 17, 2007; revised August 21, 2007. This work was supported in part by the SETI Institute, Mountain View, CA; The Ohio State University, Columbus, OH; and in part by the North American Astrophysical Observatory (NAAPO), Columbus, OH.

S. W. Ellingson is with the Bradley Department of Electrical and Computer Engineering, Virginia Polytechnic Institute and State University, Blacksburg, VA 24061 USA (e-mail: ellingson@vt.edu).

G. A. Hampson is with CSIRO-Australia National Telescope Facility, Epping NSW 1710, Australia (e-mail: Grant.Hampson@csiro.au).

R. K. Childers is with the Department of Psychology, The Ohio State University, Columbus, OH 43210 USA (e-mail: childers.2@osu.edu).

Color versions of one or more of the figures in this paper are available online at http://ieeexplore.ieee.org.

Digital Object Identifier 10.1109/TAP.2007.915467

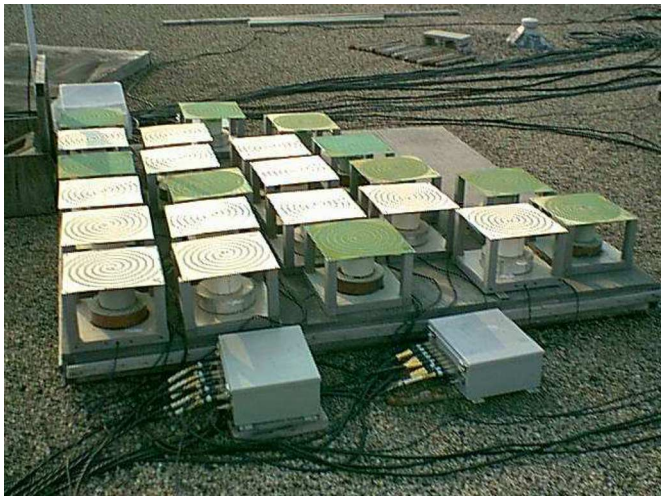

Fig. 1. The antenna array. Elements rest on a platform covered in fine wire mesh which serves as a larger ground screen. Each of the two gray boxes in the foreground contain line amps for 8 antennas (a third box is located on the far side of the array). The base of the calibration source mast is visible in the upper left. One of the 23 elements shown is currently not working.

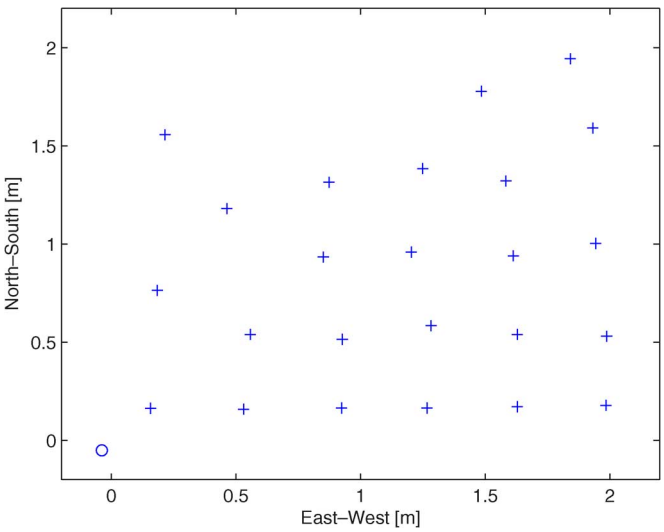

Fig. 2. The array geometry, as seen from above. The location of the calibration source is marked with a "o." The height of the source is 1.72 m with respect to the plane of the array.

about 2 m across, resulting in beamwidth $\sim 6^\circ$ at the zenith at 1700 MHz (the highest frequency of operation). The beamwidth increases with decreasing frequency and with decreasing elevation due to the planar geometry of the array.

The requirements for antenna elements used in this array are: 1) broad impedance bandwidth; 2) very broad, slowly varying antenna pattern; 3) low sensitivity to ground noise pickup, in order to reduce system temperature; and 4) low horizon gain, in order to reduce exposure to terrestrial radio frequency interference. Also, mechanical simplicity and low cost are desired. Log periodic yagis and conical spirals are obvious choices with respect the broadband requirement, but fare less well with respect to the other requirements. Instead, we chose to use planar Archimedean spirals. These are more difficult to make broadband, and have the serious problem that they produce a equal-gain backlobe, but are attractive in most other respects

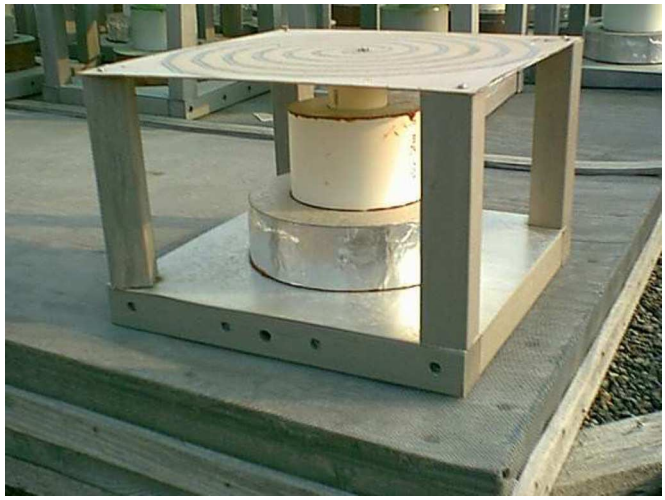

Fig. 3. Side view of a spiral antenna element.

[8]. A popular and frequency-independent scheme to suppress the backlobe is to employ an absorber-backed cavity; however this results in an unacceptable increase in system temperature in our application. It is also well-known that the backlobe can be losslessly-mitigated with ground screen one-quarter wavelength below the spiral [9]; however this obviously is a frequency-dependent solution. We chose to pursue a modification of the ground plane strategy in order to overcome this problem.

A close-up of a single Argus antenna, including the modified ground plane, is shown in Fig. 3. The spiral itself is a right-hand-circularly polarized Archimedean spiral with diameter 30 cm, printed on fiberglass epoxy (FR4) printed circuit board (PCB) material. Our design uses a tiered ground plane. The bottom ground plane measures 30 cm square and is located 17.2 cm below the spiral. Additional circular ground planes are located 12.3 cm and 5.3 cm below the spiral, having diameters 18.8 cm and 11.2 cm, respectively. This can be viewed as an approximation to a conical ground plane, where the distance to the "ground cone" is about one-quarter wavelength below the active region of the spiral, which is known to be a circle about one wavelength in circumference. The ground plane geometry used here was designed by trial and error, with the number of tiers being a tradeoff between the quality of the conical ground plane approximation and complexity. The conducting baffle (the cylindrical section between the lowest 2 ground planes) was found to significantly improve the impedance bandwidth, which is approximately 700–1700 MHz for $\mathrm{VSWR} < 1.8 : 1$ as shown in Fig. 4. The free-space pattern of the antenna (including the tiered ground plane) at 1420 MHz is shown in Fig. 5. The pattern in the lower half-space is obviously completely suppressed once the antenna is installed on the array ground plane. The typical half-power beamwidth of the antenna *in situ* is $\sim 100^\circ$ and the horizon gain is $\sim$15 dB down from zenith gain over the tuning range.

Mutual coupling can affect the performance of beamforming and direction finding for antenna arrays with spacings on the order of wavelengths, as is the case for Argus. Although we have never explicitly characterized coupling within the

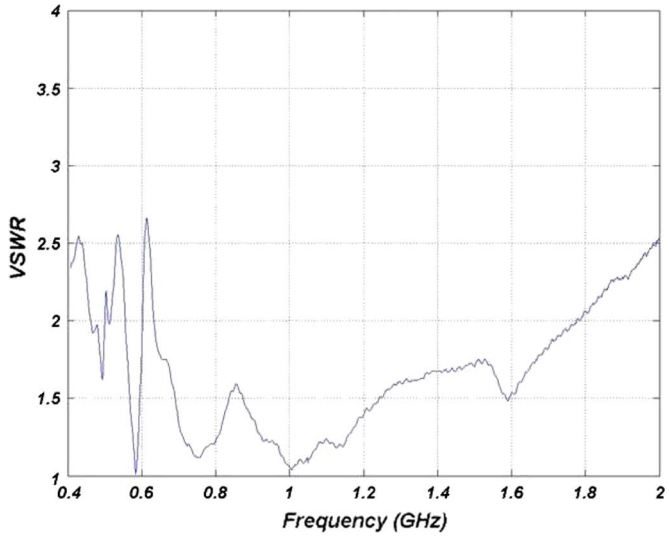

Fig. 4. Measured VSWR of antenna element, including balun.

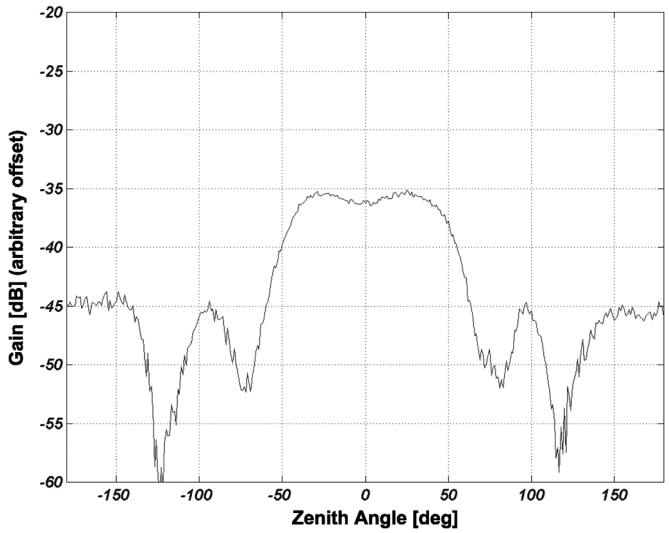

Fig. 5. Measured pattern of antenna element in free space at 1420 MHz.

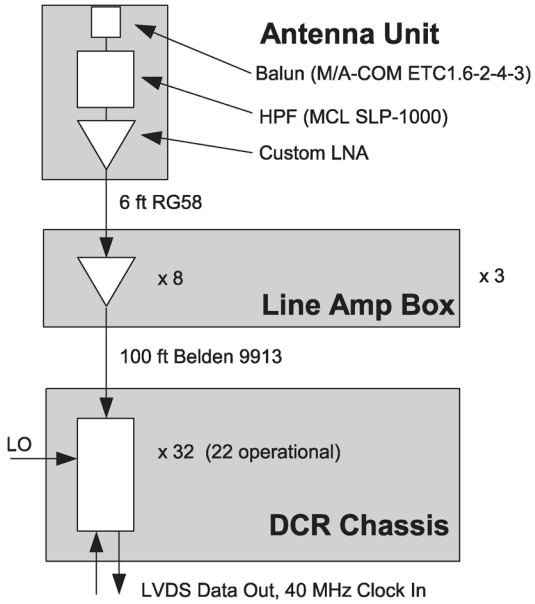

Fig. 6. Signal flow through the analog electronics.

array, the quality of the direction-finding results shown in Section IV—obtained using calibration techniques which neglect mutual coupling—indicate that coupling effects are negligible in this application, at least at the frequencies at which we have conducted these observations.

The antenna terminals are connected to a surface-mount broadband transformer (M/A-COM Model ETC1.6-4-2-3) mounted on the underside of the PCB. The transformer serves as a 4:1 balun (transforming the spiral's balanced impedance of about 200 Ω to 50 Ω single-ended) and terminates into a coaxial SMA connector.

B. Analog Electronics

Fig. 6 shows the signal flow through the analog electronics. The shaft running through the center of the antenna (visible in Fig. 3) contains a custom-designed uncooled low-noise amplifier (LNA) using the Agilent ATF-34143 PHEMT. This LNA achieves about 15 dB gain, 170°K noise temperature, and an input 1-dB compression point of -5 dBm over the bandwidth of the antenna. The overall single-antenna system temperature (including $\sim$45 K ground noise pickup through the antenna) has been determined experimentally to be about 215 K in this configuration. Shortly after commissioning the instrument, an additional coaxial highpass filter (Mini-Circuits Model SHP-1000) was inserted between the antenna and LNA to mitigate troublesome intermittent out-of-band interference. This contributes an additional 35 K, degrading the per-element system temperature $T_{\rm sys}$ to its current value of about 250 K.

The output of the antenna unit is routed via a short section of RG-58 coaxial cable to a nearby line amplifier (also of custom design), which provides an additional 20 dB gain, includes a microstrip 1200–1700 MHz bandpass filter, and powers the LNA via a bias-tee arrangement. The line amps are packaged together in groups of 8 (see Fig. 1). The line amp output is connected to remaining electronics (located indoors) via 100 ft sections of Belden 9913 coaxial cable.

A custom-designed direct conversion receiver (DCR), shown in Fig. 7, is used to convert a 14-MHz swath of spectrum from within the L-band tuning range into a complex-valued digital signal consisting of 8-bit + 8-bit samples at 20 million samples per second (MSPS) using a dual analog-to-digital converter (ADC) IC. This in turn is converted into a 320 Mb/s serial data stream for transmission using low-voltage differential signaling (LVDS). The LVDS output signal from each DCR is carried using off-the-shelf CAT5 ethernet cable.

C. Digital Electronics

Fig. 8 shows the signal flow through the digital electronics. A custom-designed "digital receiver processor" (DRP) accepts the output from a DCR and selects a swath of about 60 kHz from the 14 MHz passband for further processing. This is done using the Analog Devices AD6620 IC, which tunes the desired frequency to zero Hz, applies a digital filter to the result, and decimates the

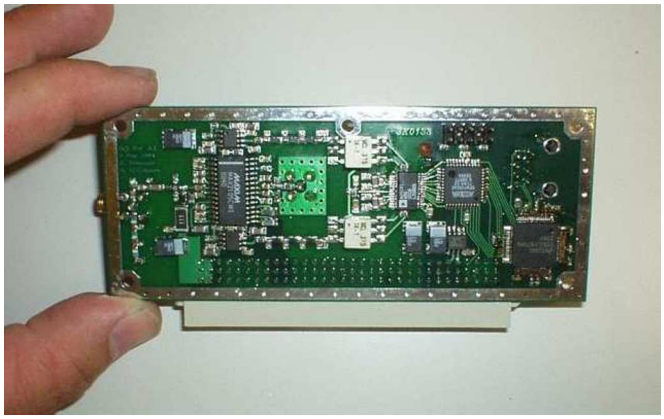

Fig. 7. DCR. Left to right: High-pass diplexer, Maxim MAX2105 direct conversion IC, Texas Instruments OPA643 IC output buffers, 7 MHz low-pass filters, baluns, Analog Devices AD9281 ADC, FPGA, LVDS transceiver IC. Jacks for RF, LO, and LVDS are on the opposite side of the board, which also forms one side of an enclosure. The enclosure is completed by an EMI shield, removed for this photo.

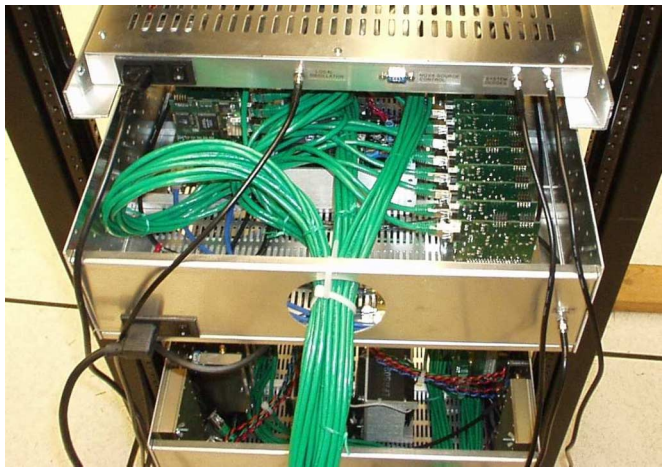

Fig. 9. A view of the electronics rack intended to provide some sense of size. The large chassis in the center and bottom contain the DRPs and DCRs respectively. The green cables connect DCRs to DRPs.

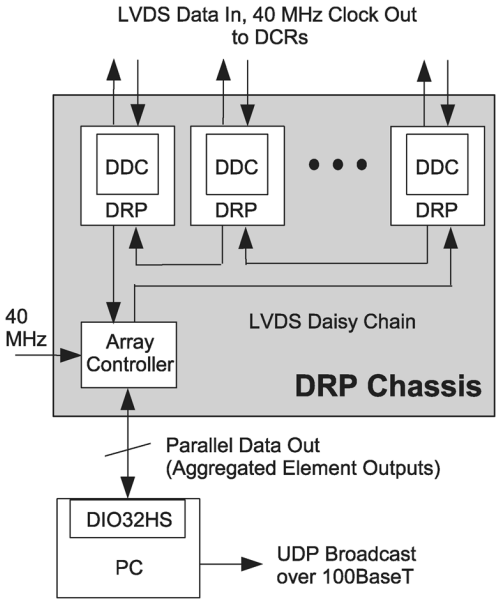

Fig. 8. Signal flow through the digital electronics.

sample rate by a factor of 256 to 78.125 thousand samples per second (kSPS).

To organize the DRP output samples into snapshots (i.e., vectors of array outputs), a serial bus "daisy chain" architecture is used. The DRPs are connected in series by LVDS links via a custom-designed backplane. Each DRP receives all the samples output by the DRPs before it, adds its output sample, and passes along the set to the next DRP. Also part of the daisy chain is an array controller card which manages the operation of the daisy chain. The aggregated data rate becomes 81.92 Mb/s. The array controller card collects the snapshots assembled using the daisy chain and outputs them in 16-bit parallel fashion. The 40 MHz system clock is received through the array controller, distributed to DRPs via the backplane, and forwarded to DCRs using a separate pair of conductors on the same cable used to transfer data in the opposite direction. Fig. 9 shows the physical arrangement.

The data words are received via a National Instruments DIO32HS board mounted in a PCI slot in a Windows 98 PC. Using a C-Language program, a "data block" of 16,384 (i.e., 16K) array snapshots, representing 209 ms in real time, is gathered and organized into data packets. These packets are relayed to a 100baseT ethernet card (also on the PCI backplane) and broadcast across a dedicated LAN using UDP/IP broadcast at 81.92 Mb/s. Currently an old PC is used which limits the duty cycle of observation to roughly 20%, and the data can be processed by a single PC. However, using a technique developed and demonstrated in [10], the system is able to accommodate any number of data processing PCs. The cluster is organized such that the PCs can take turns accepting the 16 K data blocks from the UDP/IP broadcast to sustain continuous processing, or can be used to processes the same data blocks in multiple different ways.

D. Data Analysis

Although the raw data blocks can be acquired and archived indefinitely, it is desirable to analyze the data in real time so as to facilitate immediate responses to detected transient events. An obvious approach to data analysis is simply to compute a "basis set" of N beams (where N is the number of elements) which tessellate the sky, and then to use traditional methods [11] to detect time-domain signals in the beam outputs. However, this has the serious drawback of requiring that the array be continuously and accurately calibrated. The desired calibration consists of a measurement of the *array manifold*; that is, the response of the system to a plane wave arriving from every possible direction of arrival ψ, where ψ is in the range $\{0 \leq \theta \leq \pi/2, 0 \leq \phi \leq 2\pi\}$, θ corresponds to zenith angle, and ϕ corresponds to azimuth. Calibration of any large distributed array is difficult for many reasons; for example, the element patterns are not accurately known, the gains and phases of individual elements vary independently in response to environmental changes, and so on. For Argus on the scale implemented here, it turns out that the array is too large to be measured with precision using by direct methods

(e.g., local reference signals), yet too small (insufficient sensitivity) to reliably use astronomical signals as sources. This motivates the use of detection algorithms which do not require accurate calibration.

Our current philosophy for calibration-independent detection is described in [12]. We search for broadband (astronomical) signals using an algorithm we refer to as "TXE," standing for "time-gate, cross-correlation, and eigenanalysis." Let the elements of the $N\times 1$ vector $\mathbf{x_i}$ represent the complex-valued baseband element voltages at time index i. A spatial covariance matrix is formed as follows:

$$\mathbf{R} = \frac{1}{L}\sum_{l=1}^{L} \mathbf{x}_l \mathbf{x}_l^H \tag{1}$$

where L is the number of samples and the superscript "H" denotes the conjugate transpose. A "detection metric" d_b is computed for block b as follows:

$$d_b = \lambda_1^{(b)} / \left(\mathrm{Tr}\left\{ \mathbf{R}^{(b)} \right\} - \lambda_1^{(b)} \right) \tag{2}$$

where $\mathbf{R}^{(b)}$ is $\mathbf{R}$ for block b, $\lambda_1^{(b)}$ is the primary (largest) eigenvalue of $\mathbf{R}^{(b)}$, and "$\mathrm{Tr}\{\}$" denotes the trace (sum of eigenvalues) operator. Simply put, this metric is the ratio of power in the primary eigenvalue to the remaining power incident on the array. Detection is declared when d_b exceeds a threshold number of standard deviations from its mean value over time.

The method for narrowband detections is similar, except each 16 K data block is first transformed into the frequency domain using the Fast Fourier Transform (FFT); thus, we call this algorithm "FXE." This operation is repeated for M (typically about 5) data blocks, and then the processing proceeds as in TXE except on a bin-by-bin basis. In this case, b in (2) is interpreted as frequency bin index, and the detection declared when d_b for any bin exceeds a threshold number of standard deviations from its mean value over frequency. As the data blocks are 16 K samples long at 78.125 kSPS, the bins are about 5 Hz wide.

A more detailed discussion of TXE and FXE, including analyses of performance and computational burden, is provided in [12].

E. Calibration and Localization

Detections have little value unless they can be localized so as to determine the source, or to inform traditional, more sensitive instruments where to look. To accommodate this, we maintain a coarse calibration using a noise reference calibration source mounted near the array (see Fig. 2). The source is transmitted from a small log-periodic dipole antenna pointed at the center of the array, and is activated and observed for 1 s for every 60 s of operation. (This short interval between calibration periods is in fact unnecessary as the system tends to be stable over periods on the order of hours.) We make the simplifying assumption that the element antenna patterns are identical in ψ, differing by no more than a complex constant. Under this assumption, the measurement of a single known source combined with knowledge of the array geometry is sufficient to determine the entire array manifold. This is then a simple procedure of: 1) choosing a reference element; 2) cross-correlating every other element with the reference element to determine the relative magnitude and phase; and finally 3) correcting the magnitudes and phases to account for the path loss and phase unwinding associated with the unique distance between the calibration source and each antenna. As demonstrated in Section IV, we have not found it necessary to account for mutual coupling in the array.

Localization consists of comparing the primary eigenvector—that is, the one associated with the eigenvalue which triggered the detection—to vectors corresponding to beams covering the sky. The search grid has resolution 1° in both azimuth and elevation, and therefore the sky is significantly oversampled with respect to the beamwidth. The comparison is essentially an inner product between the computed eigenvector and beam being considered.

III. Predicted Performance

In this section we provide a simple theoretical model for calculating rough estimates of sensitivity suitable for comparison to experimental results discussed in subsequent sections. For simplicity, let us assume the sky is well-modeled as consisting of a countable number of point sources (justified below), plus spatially-varying noise. The power spectral density (i.e., W/Hz) received by the nth antenna due to the mth source is

$$P_{n,m} = \frac{1}{2} S_m A(\psi_m) \tag{3}$$

where ψ_m denotes the position in the sky, S_m is the associated incident power flux density (i.e., $\mathrm{W m^{-2}\,Hz^{-1}}$) and $A(\psi)$ is the effective aperture of the antenna in direction ψ. The factor of 1/2 is due to the fact that we only measure one polarization, whereas the incident power is normally divided across both polarizations. Suppose we have a perfectly calibrated, alias-free array, such that we are able to point a well-formed beam in the direction of source. Since a beamformer coherently adds voltages, the power at the output of the beamformer due to source m is

$$P_m = \frac{1}{N}\left[\sum_{n=1}^{N} P_{n,m}^{1/2}\right]^2 = \frac{1}{2} S_m A(\psi_m) N \tag{4}$$

where the leading factor of $1/N$ is arbitrary but included so that the beamformer satisfies conservation of power. The beamformer output also includes noise from the receivers, from other directions in the sky, and from the warm ground. The *receiver* contribution to the noise power spectral density for a single element, referenced to the terminals of the antenna, is

$$Z_n^r = kT_{\mathrm{sys}} \tag{5}$$

where k is 1.38×10^{-23} J/K, and $T_{\mathrm{sys}} \sim 250$ K (as explained in Section II-B), Since this noise is uncorrelated between receivers, the total receiver noise power spectral density at the output of the beamformer is

$$Z_r = \frac{1}{N}\sum_{n=1}^{N} Z_n^r = kT_{\mathrm{sys}}. \tag{6}$$

Accurate estimation of the contribution from sky noise—call this Z_a—depends on the beam shape and the region of sky that it sees. In general, the noise contribution to the beamformer output due to sky noise is

$$Z_a = kT_a(\psi) \tag{7}$$

where $T_a(\psi)$ is the equivalent antenna temperature at the output of the beamformer due to these contributions. When pointing into the Galactic plane, $T_a(\psi)$ is dominated by Galactic noise and can be up to $\sim$ 100 K at some frequencies [1]. Pointing out of the plane of the Galaxy, Galactic noise is negligible and $T_a(\psi)$ instead is the sum of the cosmic microwave background (CMB) at ~3 K plus a few K associated with atmospheric losses, for <6 K total. Taking into account all these factors, and assuming the bandwidth of detection B is less than or equal to the source bandwidth, we have that the signal-to-noise ratio (SNR) for source m in the absence of any other sources is

$$\mathrm{SNR} = \frac{P_m}{Z_r + Z_a} = \frac{S_m A(\psi_m) N}{2k\left(T_{\mathrm{sys}} + T_a(\psi_m)\right)}. \tag{8}$$

Note, $T_a(\psi_m) \ll T_{\mathrm{sys}}$ and thus this term can be safely neglected. If we require $\mathrm{SNR} = 1$ for a detection, then the sensitivity of the system is given by

$$S_{\min} = \frac{2kT_{\mathrm{sys}}}{A(\psi_m)N} \frac{1}{\sqrt{B\tau}} \tag{9}$$

where we have accounted for the ability to improve sensitivity by increasing $B\tau$ from 1, by increasing the integration time τ.

It should be noted that strictly speaking (9) only applies in the special case in which the sky is dominated by one discrete source, and when the system is pointing a beam at it. An example where this is valid is for an observation of the Sun, which has $S_m \sim 3 \times 10^{-21}$ Wm^2 Hz^{-1} in L-Band normally (i.e., "Quiet Sun" conditions). In units preferred by radio astronomers, this is 300 kJy where 1 $\mathrm{Jy} = 10^{-26}\mathrm{Wm}^{-2}$ Hz^{-1}, and is at least two orders of magnitude greater than any other natural source in the sky [1].

Since the antenna elements are electrically small, they have broad patterns and therefore $A(\psi)$ varies slowly over the sky. For our antennas, the zenith value can be estimated as

$$A(0) = \epsilon \frac{\lambda^2}{4\pi} D \tag{10}$$

where the directivity D can be crudely estimated as being about 2, and the efficiency ϵ (accounting for imperfect VSWR and ohmic losses) averages about 0.86. At 1700 MHz (the high end of the tuning range, at which $A(0)$ is smallest), $A(0)$ is therefore ≈ 42 cm^2. Using $N = 22$, $B = 60$ kHz, and $\tau = 209$ ms, we have $S_{\min} = 66$ kJy.

IV. Example: Tracking the Sun

The Sun appears in L-band as a point source (i.e., unresolved by the beam) of about 300 kJy, dominating over all other natural radio sources. This makes it a convenient target for confirmation of system performance. We present here an example of Argus' ability to detect, locate, and track the sun in an experiment conducted in May 2007. The observation was conducted at 1500.9 MHz. Using (9) and (10), we estimate $S_{\min} = 51$ kJy ($N = 22$, $B = 60$ kHz, and $\tau = 209$ ms), and therefore expect SNR ~6 if the sun were to reach zenith. On the date of the experiment, the maximum elevation of the sun was 67°. Assuming that the pattern of a single antenna element is proportional to $\cos^2\psi$, then we expect the SNR when the sun is at it's peak elevation to be ~5. In the results shown below, ten 209 ms observations are averaged together. This reduces the variance of the estimates, making this low SNR easier to perceive.

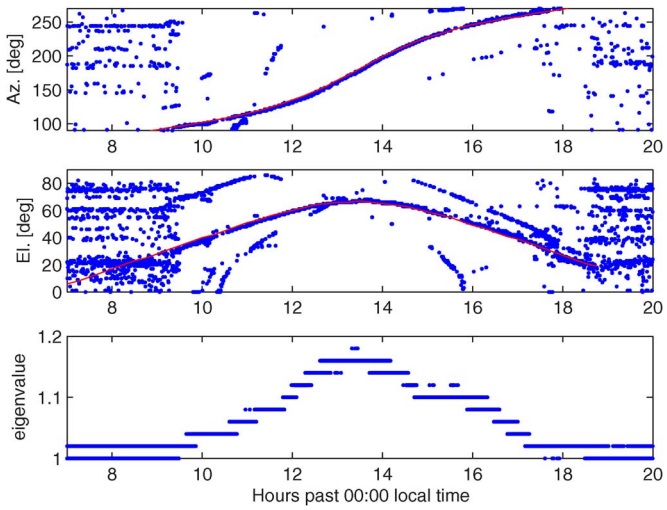

Fig. 10. Tracking the Sun: Estimated azimuth (*top*), elevation (*middle*), and primary eigenvalue, normalized such that its quiescent value is 1 (*bottom*). The solid line in the upper two plots is the actual position of the Sun taken from astronomical ephemeredes. Note eigenvalues are quantized as part of data recording; i.e., the quantization is not an artifact of the processing.

Fig. 10 summarizes the results for a day of observation. The bottom panel shows the maximum eigenvalue λ_1 of the spatial covariance matrix $\mathbf{R}$, divided by the sum of eigenvalues and further normalized to its mean quiescent (night time) value. This result can be used to confirm that the instrument detects the sun with the expected sensitivity, as follows: Note that λ_1 rises from 1 to its maximum value of 1.18, and then declines to 1 again in the manner expected for the Sun observed over the course of the day. This variation compares favorably to the expected value, assuming peak $\mathrm{SNR} = 5$, of

$$\frac{5 + \sum_{n=1}^{N} 1}{\sum_{n=1}^{N} 1} = 1.23. \tag{11}$$

The error compared to prediction can be attributed to a combination of uncertainty in solar flux and antenna patterns.

The upper panels of Fig. 10 show system-generated estimates of azimuth and elevation as a function of local time. In these plots, each point is an estimate generated using the TXE algorithm described in Section II-D. The number of outliers is relatively small given the low SNR. The values of the outliers are a deterministic artifact of the eigenstructure-based direction-finding algorithm (associated with calibration error), and do not necessarily represent signals received through physical

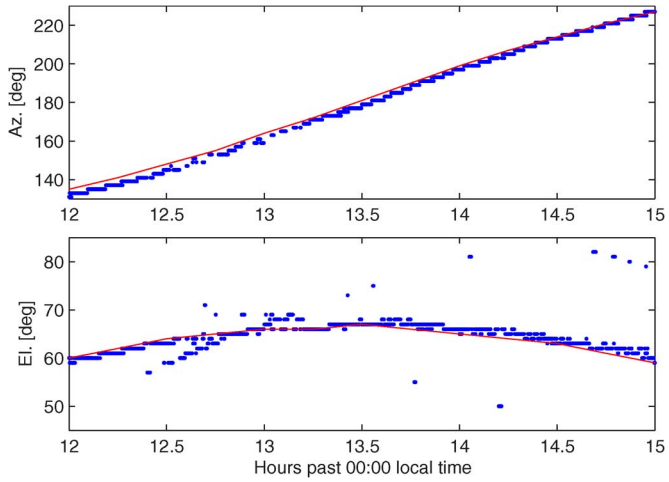

Fig. 11. Close-up of the upper two panels of Fig. 10.

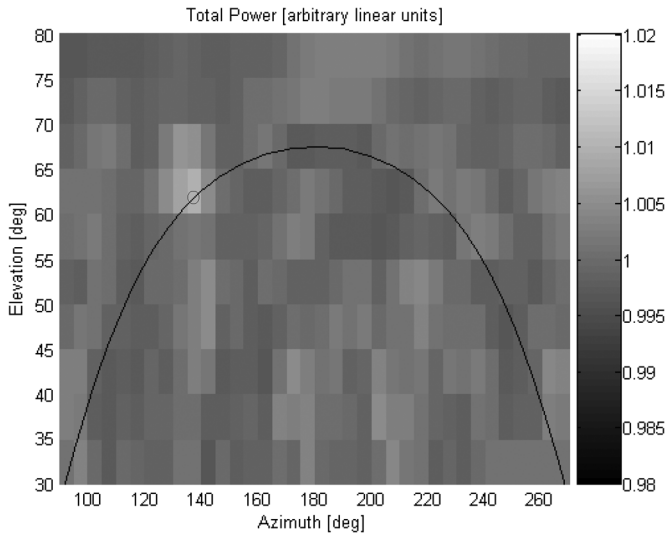

Fig. 12. A radio map of the southern sky formed by pointing a beam at each position in a $5^\circ \times 5^\circ$ grid. The sun is visible at about 140° azimuth and 60° elevation. The track of the sun, taken from solar ephemeredes, is shown as a solid black line with the position at the time of the data collection shown as a small circle.

sidelobes. Before sunrise and after sunset, the estimates are essentially random but tend to form clusters because the crude calibration results in a noise covariance which is not perfectly "white."

Fig. 11 shows a close-up of the same data presented in the top two panels of Fig. 10, around the time at which the sun is near its maximum elevation, demonstrating the low bias and variance of the estimates.

Fig. 12 shows a map of the sky formed by computing the total power in beams pointed according to a grid having spacings $5^\circ \times 5^\circ$. This image confirms the dominance of the sun in the sky and is consistent with the predicted and estimated SNR.

V. Other Experiments and Results

We have performed a number of additional experiments demonstrating various capabilities of Argus. These are summarized below.

A. Blind Detection of Satellite Interferers

In [13], we reported an experiment in which demonstrated Argus' ability to "blindly" detect signals from man-made satellites. In this case, "blind detection" refers to detection using TXE/FXE with no calibration of the array beyond gain-leveling of the elements. First we observed at 1691.00 MHz, corresponding to the weather fax (WEFAX) signal from the GOES-12 satellite [14]. GOES-12 is geostationary and appears fixed in the sky at a position of (from Columbus, OH) 168° north azimuth and 43° elevation. (A related satellite, GOES-10, transmits on the same frequency but appears only 19° above the horizon and thus is effectively squelched by a combination of increased path loss and element antenna patterns.) In this case, Argus correctly determined the presence of 1 signal. Then we observed at 1691.03 MHz, which is nominally signal-free, and Argus correctly determined no significant detections. Finally, we observed at 1575.42 MHz, the center frequency of the L1 signal transmit from the U.S. Global Positioning System (GPS) constellation of satellites [15]. Typically, eight to ten GPS satellites are above the horizon at any given time; three to four of these should be within the 3 dB beamwidth of the Argus elements, whereas an additional three to six satellites should be high enough in elevation to be detectable. The dominant C/A component transmitted from each GPS satellite is incident with flux density $\sim$20 MJy in $\sim$1 MHz, which amounts to about four times stronger than the Sun with respect to the Argus receiver bandwidth. In our experiment, nine signals were detected.

In addition to being useful diagnostics, experiments such as these suggest other possible applications of this technology including automated detection and tracking of space-borne radio frequency interference in support of traditional radio astronomy.

B. Transient Detection by All Sky Imaging

Also in [13], we demonstrated the ability of Argus to perform sensitive all-sky imaging, which is an alternative, useful method for transient detection. In this approach, transients are detected by comparing sky images taken at different times. Again, the 1691 MHz WEFAX signal from GOES 12 was used. To form the image, we constructed the array covariance matrix $\mathbf{R}$ from the inter-element correlations (as usual) and then computed the image as the angle power spectrum $\mathbf{a}^H(\psi)\mathbf{R}\mathbf{a}(\psi)$ where $\mathbf{a}(\psi)$ is the assumed array manifold sampled at ψ. Images showing the sky at 1691.00 MHz (showing the WEFAX emission emanating from a point source in the sky), and 1691.03 (exhibiting no such point source) are presented in [13].

C. Interference Mitigation

In [16], we demonstrated the ability of Argus to perform sensitive spectroscopy at 1624 MHz in the presence of transmissions from the Iridium constellation of satellites [17]. Iridium produces short burst transmissions. We employed two methods to mitigate the pulses: time window blanking, and adaptive sidelobe canceling. It was shown that blanking was extremely effective in mitigating Iridium bursts, but with about 20% loss of data, i.e., reduced effective integration time. Adaptive sidelobe canceling entailed no loss of data, but was limited to about 30 dB suppression.

In [12], we described another form of RFI mitigation that could be integrated into TXE/FXE to mitigate spurious detections; however this approach is not currently implemented.

VI. Current Status and Implications for Future Work

Argus continues to operate continuously except for occasional short breaks for maintenance. Since 2004, the narrowband and broadband search algorithms are used, with detection metrics and associated beam data being computed and saved. This is sufficient to check retroactively for associations with strong astronomical transients detected using other means, e.g., satellite-based Gamma-ray observatories. In January 2007, we implemented a feature in which all raw data from the array are recorded continuously for 5 min in response to sufficiently strong detections, facilitating extensive post-processing analysis and true "retroactive observing."

To date, the real-time processing has made no astronomically-significant detections beyond those associated with the Sun (which *frequently* creates interesting transients) and man-made satellites. It is possible that our data archive contains significant events which could be identified through associations with other known astronomical transient events, periodicity searches, or various other "data mining" techniques to improve sensitivity. Also, we are working to expand the number of operational elements in the array from the current 22 to the full complement of 32 supported by the current design.

To our knowledge, Argus remains unique in its capabilities, at least in its frequency range. A project similar enough to worth noting is the Thousand Element Array (THEA) of Astron (The Netherlands) [18]. THEA consists of four tiles of 64 Nyquist-spaced, single-polarization Vivaldi elements (i.e., 256 elements total) which operate from 600 MHz to 1700 MHz. THEA is claimed to have 40 K LNAs resulting in per-element $T_{\rm sys} = 150\ {\rm K}$. Thus, THEA is significantly more sensitive than Argus. However, the beamforming architecture of THEA is hierarchical in the sense that all elements in a tile are combined first using analog beamforming, and the result is digitized. Each tile can produce only two simultaneous beams. Digital signal processing is then limited to processing of four pairs of beams, i.e., one pair from each tile. This is in contrast to Argus, in which all elements are digitized and any number of simultaneous beams can be generated, or in which all elements can simply be recorded to disk for later processing. It is also worth noting that an emerging generation of new low-frequency (<300 MHz) radio telescopes plan to include all-sky surveillance capabilities akin to those of Argus: These include the American-Australian Mileura wide-field array (MWA) low frequency demonstrator (LFD) [19], the American long wavelength array (LWA) [20] and eight-meter-wavelength transient array (ETA) [21], and the Dutch low frequency array (LOFAR) [22].

An interesting question is the number of elements a larger Argus instrument would require to have sensitivity comparable to present-day "front-line" radio telescopes. For a point of reference, the Green Bank Telescope (GBT) has a mechanically-steered 7854 $\rm m^2$ aperture and $T_{\rm sys} \approx 55\ {\rm K}$ in L-Band [23]. Argus would require about eight million elements to achieve the same sensitivity on a gain-over-temperature basis. However, it would achieve this sensitivity over entire sky, whereas the GBT achieves it only in a beam about 0.1° degrees wide. Nevertheless, it is difficult to imagine how an instrument of this scale could be realized using an architecture in which every element is digitized. Fortunately, broad classes of transient signals are known to exist which are well-suited to observation by instruments which are orders of magnitude smaller [2]. A 10,000-element Argus-type system would be sensitive to short transients on the order of 150 Jy and would be both a relatively affordable and scientifically exciting instrument.

Acknowledgment

R. S. Dixon of The Ohio State University and the volunteers of NAAPO (http://www.naapo.org), have contributed substantial material and labor support to this project. Many staff and student members of the Ohio State University ElectroScience Laboratory also made significant contributions; in particular G. Whipps and T. Alferink.

References

[1] K. Rohlfs and T. L. Wilson, *Tools of Radio Astronomy*, 3rd ed. Berlin, Germany: Springer-Verlag, 2000.

[2] J. M. Cordes, T. J. W. Lazio, and M. A. McLaughlin, "The dynamic radio sky," in *Science with the Square Kilometre Array*, C. Carilli and S. Rawlings, Eds. The Netherlands: Elsevier, Dec. 2004, vol. 48, New Astronomy Reviews.

[3] R. S. Dixon, "Argus: A next-generation omnidirectional radio telescope," in *High-Sensitivity Radio Astronomy*, N. Jackson and R. J. Davies, Eds. Cambridge, U.K.: Cambridge Univ. Press, 1997, pp. 260–268.

[4] J. Tarter, J. Dreher, S. W. Ellingson, and W. J. Welch, "Recent progress and activities in the Search for Extraterrestrial Intelligence (SETI)," in *Review of Radio Science, 1999–2002*, W. R. Stone, Ed. New York: IEEE Press/Wiley, 2002, ch. 36.

[5] R. D. Ekers, D. K. Cullers, J. Billingham, and L. K. Scheffer, Eds., *SETI 2020: A Roadmap for the Search for Extraterrestrial Intelligence*. Mountain View, CA: SETI Press, 2002.

[6] Argus Project Website [Online]. Available: http://www.ece.vt.edu/swe/argus

[7] S. W. Ellingson and G. A. Hampson, "Argus Telescope Development in 2002," The Ohio State University ElectroScience Laboratory, Tech. Rep. 531393-4, Jan. 2003.

[8] J. Kaiser, "The Archimedean two-wire spiral antenna," *IEEE Trans. Antennas Propag.*, vol. 8, no. 3, pp. 312–323, May 1960.

[9] H. Nakano, K. Nogami, S. Arai, H. Mimaki, and J. Yamauchi, "A spiral antenna backed by a conducting plane reflector," *IEEE Trans. Antennas Propag.*, vol. AP-34, no. 6, pp. 791–796, Jun. 1986.

[10] T. Alferink, "A digital signal processing engine for a large antenna array," Master's thesis, The Ohio State Univ., Columbus, 2000.

[11] S. M. Kay, *Fundamentals of Statistical Signal Processing, II: Detection Theory*. Englewood Cliffs, NJ: Prentice Hall, 1998.

[12] S. W. Ellingson, "Detection of tones and pulses using a large, uncalibrated array," in *Proc. IEEE Antennas Propagation Society Int. Symp.*, Columbus, OH, Jun. 2003, vol. 4, pp. 196–199.

[13] S. W. Ellingson and G. A. Hampson, "Detection and localization of L-band satellites using an antenna array," in *Proc. IEEE Int. Antennas Propagation Symp.*, Monterrey, CA, Jun. 2004, vol. 1, pp. 177–180.

[14] Loral Space Systems, GOES I-M DataBook, (DRL 101-08) Rev. 1, Aug. 31, 1996.

[15] E. D. Kaplan, Ed., *Understanding GPS: Principles and Applications*. Boston, MA: Artech House, 1996.

[16] S. Ellingson and P. McDougle, "Iridium: Characterization and countermeasures," in *Workshop on Mitigation of Radio Frequency Interference in Radio Astronomy (RFI2004)*, Penticton, BC, 2004 [Online]. Available: http://www.ece.vt.edu/swe/RFI2004

[17] Iridium Web Site [Online]. Available: http://www.iridium.com

[18] J. G. Bij de Vaate, S. J. Wijnholds, and J. D. Bregman, "Two dimensional 256 element phased array system for radio astronomy," in *Proc. IEEE Int. Symp. on Phased Array Systems and Technology*, Boston, MA, Oct. 2003, pp. 359–364.

[19] Mileura widefield array (MWA) low-frequency demonstrator (LFD) [Online]. Available: http://www.haystack.mit.edu/ast/arrays/mwa/LFD
[20] Long Wavelength Array (LWA) [Online]. Available: http://lwa.unm.edu
[21] Eight-Meter-Wavelength Transient Array (ETA) [Online]. Available: http://www.ece.vt.edu/swe/eta
[22] Low Frequency Array (LOFAR) [Online]. Available: http://www.lofar.org
[23] Green Bank Telescope (GBT) [Online]. Available: http://www.gb.nrao.edu/gbt

Steven W. Ellingson (S'87–M'90–SM'03) received the B.S. degree in electrical and computer engineering from Clarkson University, Potsdam, NY, in 1987, and the M.S. and Ph.D. degrees in electrical engineering from The Ohio State University, Columbus, in 1989 and 2000, respectively.

From 1989 to 1993, he served on active duty with the U.S. Army. From 1993 to 1995, he was a Senior Consultant with Booz-Allen and Hamilton, McLean, VA. From 1995 to 1997, he was a Senior Systems Engineer with Raytheon E-Systems, Falls Church, VA. From 1997 to 2003, he was a Research Scientist with the Ohio State University ElectroScience Laboratory. Since 2003, he has been an Assistant Professor in the Bradley Department of Electrical and Computer Engineering at Virginia Polytechnic Institute and State University. His research interests include antennas and propagation, applied signal processing, and instrumentation.

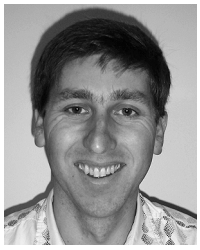

Grant A. Hampson received the B.Sc. and Ph.D. degrees in computing from Monash University, Melbourne, Australia, in 1993 and 1997, respectively.

He was an SKA Postdoctoral Researcher with the Netherlands Foundation for Research in Astronomy, Dwingeloo, The Netherlands, from 1997 to 2001. From 2001 to 2004, he was a Research Scientist with the Ohio State University ElectroScience Laboratory, Columbus. Since 2004, he has been with the CSIRO-Australia Telescope National Facility, Epping NSW, as a Research Engineer. His research interests include wide bandwidth digital signal processing and pulsar astronomy instrumentation.

Russell K. Childers received the B.S. and M.S. degrees in electrical engineering from The Ohio State University, Columbus, in 1987 and 1993, respectively.

From 1989 to 1997, he was Chief Observer at the Ohio State University Radio Observatory, where, since 2003, he has been Chief Engineer and Chief Observer at the Ohio Argus Array Radio Observatory. He is also a Programmer/Engineer at The Ohio State University.